# Temperature measurements in a string of three closely spaced droplets before the start of puffing/micro-explosion: Experimental results and modelling

D.V. Antonov, R.S. Volkov, R.M. Fedorenko, P.A. Strizhak, Guillaume Castanet, S.S. Sazhin

# Temperature measurements in a string of three closely spaced droplets before the start of puffing/micro-explosion: Experimental results and modelling

D.V. Antonov[a], R.S. Volkov[a], R.M. Fedorenko[a], P.A. Strizhak[a], G. Castanet[b], S.S. Sazhin[c,d,*]

[a] National Research Tomsk Polytechnic University, 30, Lenin Avenue, Tomsk, 634050, Russia
[b] Université de Lorraine, CNRS-UMR7563, CS 25233, France
[c] Advanced Engineering Centre, University of Brighton, Brighton, BN2 4GJ, UK
[d] Samara National Research University, 34, Moskovskoye Shosse, Samara 443086, Russia

*Keywords:*
Composite droplets
Puffing
Micro-explosion
Heating
Evaporation
Droplets in a row

A B S T R A C T

The results of experimental and theoretical investigation of the mutual effects of three composite Diesel fuel/water droplets, one behind the other, on their puffing/micro-explosion are presented. The analysis is focused not only on finding the time instant when puffing/micro-explosion starts, but also on the investigation of time evolution of temperature at the water-fuel interface before the development of puffing/micro-explosion. The experimentally observed temperatures at the water-fuel interface are shown to increase almost linearly with time for the lead, middle and downstream droplets. Assuming that puffing/micro-explosion starts when the temperature at this interface reaches the water nucleation temperature, the values of the latter temperature as a function of the heating rate were found from the experimental data. The results are shown to be consistent with the earlier found correlation for this temperature for all three droplets. Time to puffing/micro-explosion is shown to decrease with increasing gas temperature; this time for the lead droplet is always shorter than that of the middle and downstream droplets, and the difference between them decreases as the distance between droplets increases. The experimental results are interpreted in terms of the previously developed model based on the assumption that the water sub-droplet is located exactly in the centre of the Diesel fuel droplet and that this process is triggered when the temperature at the water/fuel interface attains the water nucleation temperature. The effect of interaction between lead, middle and downstream droplets is considered via modifications to the Nusselt ($Nu$) and Sherwood ($Sh$) numbers for these droplets due to the interaction between them.

## 1. Introduction

Adding water into fuel droplets is known to lead to their puffing (swelling of droplets and their disintegration into a relatively small number of smaller droplets) and/or micro-explosion (disintegration of droplets leading to the formation of a cloud of aerosols). Practical engineering applications of these processes, including those in Diesel engines, are well known [1]. These processes have been extensively studied experimentally. Among numerous papers focused on this topic we can mention [2], where the effects of various physical properties on the occurrence of micro-explosions are described, and [3,4], where the results of investigation of the effects of ambient temperatures on micro-explosions are presented. The authors of [5,6] described the results of their experimental investigation of fuel composition on puffing and micro-explosion. As follows from the parametric study of the occurrence of micro-explosions in water-in-oil emulsions presented in [7], this phenomenon is more likely to occur in larger droplets (with diameters above 20 μm) than in smaller droplets. The effects of coalescence of the dispersed water droplets on the occurrence of micro-explosions were investigated experimentally by the authors of [8,9].

The most advanced models of puffing and micro-explosion developed so far are based on Direct Numerical Simulation [10–12]. These were complemented by several simplified models of the phenomena [13–17]. The latter model and its recent modifications (e.g. [18]) has proven to be effective for the analysis of various observations of puffing and micro-explosion. It will be used in the present analysis.

In our previous paper [19], we presented the results of the experimental and theoretical investigations of the mutual effect of

* Corresponding author.
*E-mail address:* s.sazhin@brighton.ac.uk (S.S. Sazhin).

**Nomenclature**

| | |
|---|---|
| $B_{M(T)}$ | Spalding mass (heat) transfer number [-] |
| $C$ | Distance parameter[-] |
| $L$ | Distance between droplets [m] |
| $n$ | number of measurements [-] |
| $Nu$ | Nusselt number [-] |
| $Pr$ | Prandtl number [-] |
| $R$ | Distance from the droplet centre [m] |
| $R_{d0}$ | Initial droplet radius [m] |
| $Re$ | Reynolds number [-] |
| $S$ | Root squared deviation [m or s] |
| $Sc$ | Schmidt number [-] |
| $Sh$ | Sherwood number [-] |
| $t$ | Time [s] or Student's coefficient [-] |
| $T$ | Temperature [°C or K] |
| $Y$ | Mass fraction [-] |

*Greek symbols*

| | |
|---|---|
| $\alpha_c$ | Confidence level [-] |
| $\alpha, \beta, \delta, \gamma$ | Coefficients introduced in Eqs. (2) and (3) [-] |
| $\Delta_r$ | Random errors [m or s] |
| $\Delta T_{SH}$ | The degree of super-heating [K] |
| $\tau_p$ | Time to puffing/micro-explosion [s] |

*Subscripts*

| | |
|---|---|
| $B$ | Boiling |
| $d$ | Droplet |
| gas | Ambient gas (air) |
| iso | Isolated |
| $N$ | Nucleation |
| $S$ | Surface |
| $SH$ | Super-heat |
| $v$ | Vapour |
| $w$ | Water-fuel interface |
| 0 | Initial |
| $\infty$ | Ambient conditions |

droplets on their puffing/micro-explosion in a flow, using an example of two closely spaced composite rapeseed oil/water droplets in tandem. This paper is focused on the generalisation of the results of [19] in the following three directions. Firstly, in contrast to [19] we consider not two but three droplets, one behind the other. Secondly, we consider not rapeseed oil/water but Diesel fuel/water droplets in a wide range of fuel and water volume fractions. Thirdly, the focus of our analysis is not only on finding the time instant when puffing/micro-explosion starts, but also on the investigation of time evolution of temperature at the fuel-water interface before the development of puffing/micro-explosion.

The analysis of three droplets instead of two will allow us to perform more realistic investigation of the effects of surrounding droplets on any particular droplet in a spray. In this case, we will be able to consider not only the influence of the droplet in front of a given droplet but also the one behind it at the same time (cf. the results of a similar investigation presented in [20,21]).

The following volume fractions of Diesel fuel and water were used in the experiments: 90% Diesel fuel/10% water and 10% Diesel fuel/90% water, although most attention is focused on the former case. Droplets with high volume fractions of Diesel fuel are widely used in various spray combustion devices [22,23], while those with low volume fractions of Diesel fuel are used for thermal and fire purification of liquids [24,25]. In both cases, a water sub-droplet is located inside a Diesel fuel droplet.

The main features of the experimental setup and procedure used in our analysis are summarised in Section 2. The new experimental results are presented in Section 3. In Section 4 an overview of the model used in the analysis is presented. This includes a summary of the model developed in [17] and the results of investigation of the mutual effects of three droplets, one behind the other, on the values of Nusselt ($Nu$) and Sherwood ($Sh$) numbers. The model described in Section 4 is used for the analysis of experimental data presented in Section 3. The results are presented in Section 5. In Section 6 the key results of the paper are summarised.

## 2. Experimental setup and procedure

The experimental setup and methodology used in our analysis are essentially the same as described in [19] except that an opening was drilled in the metal cylinder to allow droplet illumination by a laser beam. The temperature profiles in the droplets were obtained using the Planar Laser Induced Fluorescence (PLIF) method following the methodology described in [26]. In contrast to [26], the PLIF measurements in our experiments were performed using a Phantom MIRO M310 video camera (monochromic images with maximal resolution 1280 pixels × 800 pixels, $6.5 \times 10^5$ fps, 12 bit depth) and continuous DPSS laser KLM-V532/h-10000 (wave length 532 nm; width of the spectral line 0.1 nm; maximal power 10 W with fluctuations not exceeding 5%; aperture beam diameter 3 mm).

The three droplets were mounted as shown in Fig. 1. The droplets shown in this figure are illuminated by the laser beam which leads to yellow light emission around them generated by Rhodamine B dye. Ambient gas temperature and velocity used in the experiments were in the range 589–629 K, and 0.1 m/s, respectively. The systematic errors of the measurement of these parameters were ±3 K and ±0.05 m/s, respectively.

Droplet initial radii and the distances between droplets were determined with systematic errors not exceeding ±0.025 mm and ±0.05 mm, respectively.

The results of calibration of fluoroform Rhodamine B emission intensity versus droplet temperature (measured using a thermocouple) are presented in Fig. 2. These results were approximated by the calibration curve: Intensity $= aT_d^2 + bT_d + c$, where $a = 5.86 \times 10^{-3}$; $b = -4.6568$; $c = 9.2542 \times 10^2$.

The time instant when puffing/micro-explosion started was determined by analysing video frames of the process and identifying the frame in which the first fragment separated from the main droplet. Thus, the systematic error of determining the time to puffing was equal to the time interval between frames which was 1 ms in our experiments.

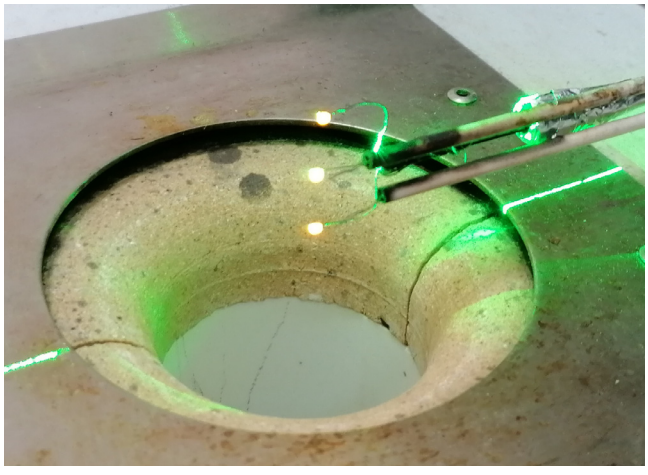

**Fig. 1.** An image of the group of three droplets used in our experiments.

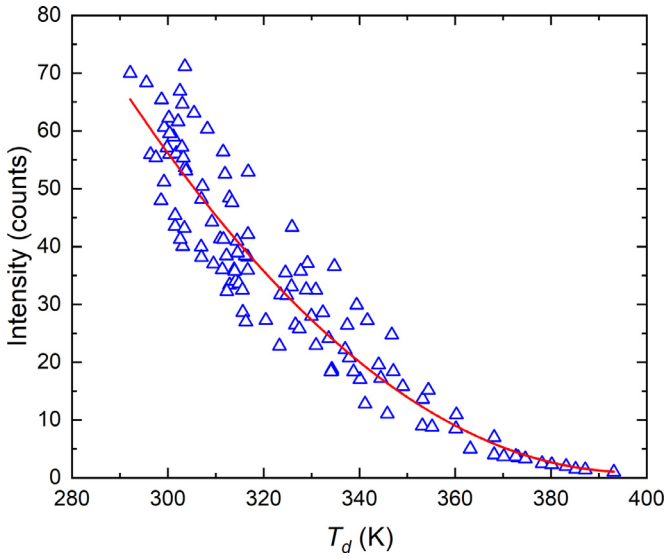


**Fig. 2.** The results of calibration of fluoroform Rhodamine B emission intensity versus droplet temperature (symbols) and the approximation of these results (calibration curve; solid curve). Random error in plotting the calibration curve did not exceed 9 K.

The analysis of images was carried out following the scheme presented in Fig. 3, using algorithm DaVis v. 10.0.5.42579. Firstly, the smoothing of images using the linear filter was performed in areas of 3 pixels × 3 pixels. The difference in the intensity of the laser beam at its centre and at the periphery was taken into account based on an analysis of the emission intensity in a cuvette filled with Rhodamine B solution. The background was removed using a procedure called 'add algorithmic mask'. Finally, the temperature field was obtained using the calibration curve shown in Fig. 2.

Pixels with unwanted fluorescence values were set to zero intensity in all the video frames (algorithmic masks), as in our previous papers [27,28]. The mean fluorescence intensity of water sub-droplets was determined in the selected recording area within 10 to 15 frames. The mean fluorescence intensity of water sub-droplets containing Rhodamine B was between 3 and 50 counts. The background fluorescence intensity ranged from 0 to 2 counts depending on the frame region.

A resolution of 384 pixels × 800 pixels was used in the experiments. This resolution remained unchanged during the filtration process.

The error bars shown in the figures are the sums of systematic and random errors. Random errors $\Delta_r$ were determined as:

$$\Delta_r = t(\alpha_c, n)S,$$

where $t(\alpha_c, n)$ is the Student's coefficient, depending on the number of measurements $n$ and confidence level $\alpha_c$, assumed equal to 0.95; $S$ is the root squared deviation for a series of measurements.

## 3. Experimental results

Typical examples of the distribution of temperature inside the three droplets for various input parameters are shown in Figs. 4 (for droplets of 90% Diesel fuel) and 5 (for droplets of 10% Diesel fuel). Note that Rhodamine B dissolves well in water but does not dissolve in hydrocarbon fuels, including Diesel fuel. Thus the

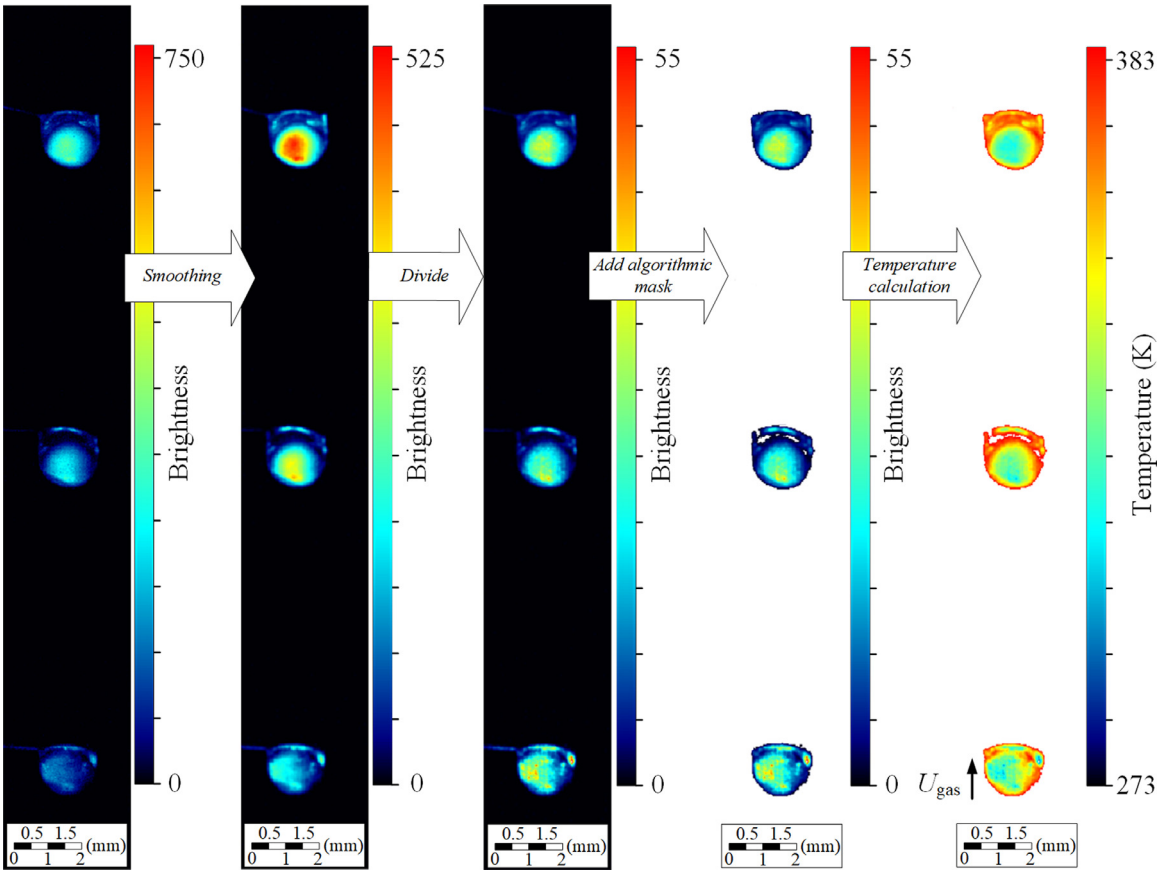


**Fig. 3.** The analysis of images performed using DaVis software.

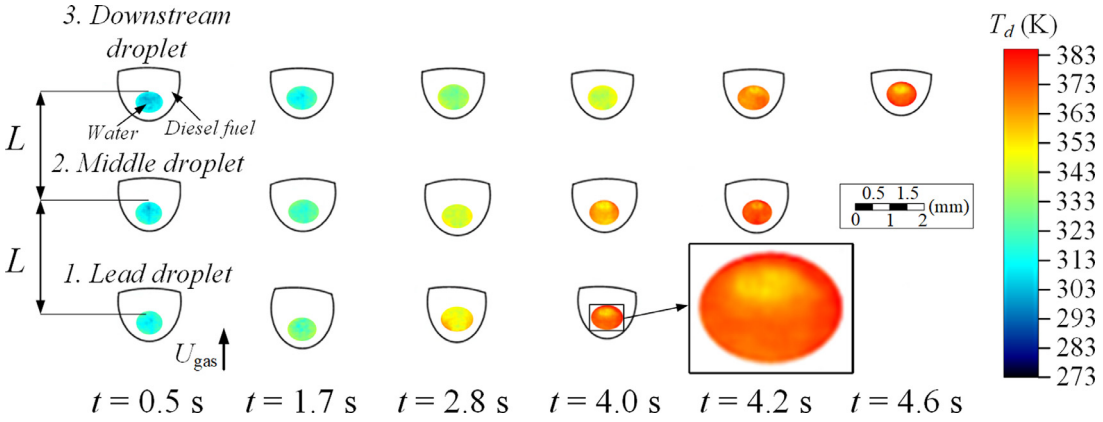


**Fig. 4.** Typical temperature fields in three droplets (volume fraction of Diesel fuel is 90%; volume fraction of water is 10%), one behind the other, for ambient gas temperature $T_{gas} = 604 \pm 10$ K, distance between droplets $L = 3.55 \pm 0.05$ mm, and initial droplet radii $R_{d0} = 0.88 \pm 0.03$ mm. The droplet boundaries are shown by the black contours.

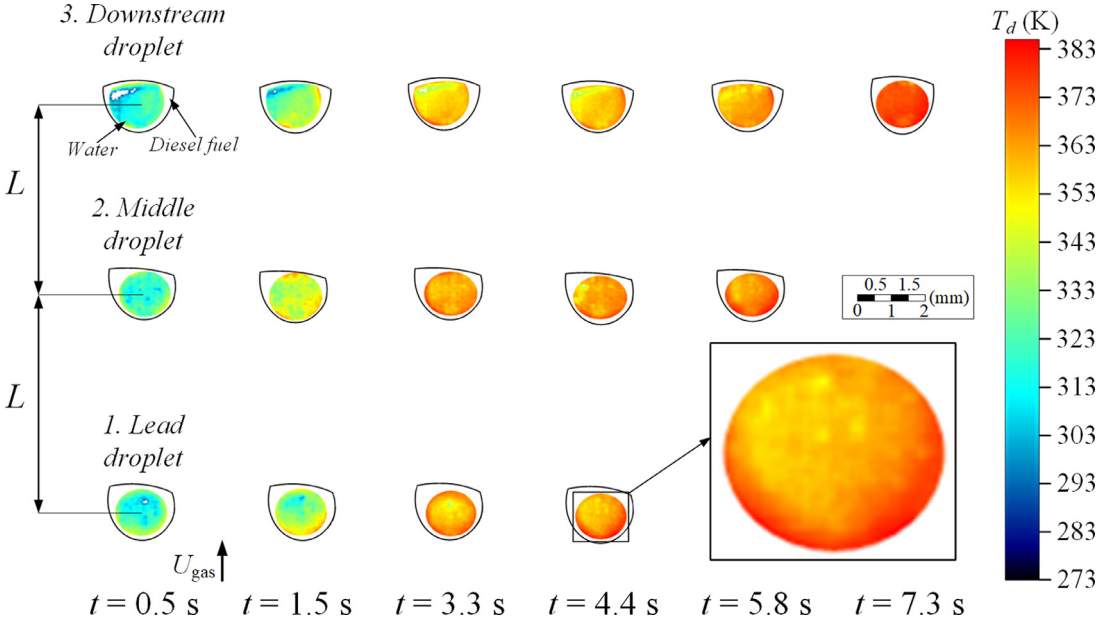


**Fig. 5.** Typical temperature fields in three droplets (volume fraction of Diesel fuel is 10%; volume fraction of water is 90%), one behind the other, for ambient gas temperature $T_{gas} = 604 \pm 10$ K, distance between droplets $L = 6.48 \pm 0.06$ mm, and initial droplet radii $R_{d0} = 0.91 \pm 0.02$ mm. The droplet boundaries are shown by the black contours.

distribution of temperature inside the droplet could only be obtained in the water sub-droplet using the PLIF method. This is well illustrated by Figs. 4 and 5.

As can be seen in Figs. 4 and 5, in all cases the lead droplet heats up faster than the middle one and the middle one heats up faster than the downstream one. The lead droplet disintegrates first, followed by the disintegration of the middle and downstream droplets. This behaviour is similar to that described in [19] for two droplets in tandem.

As follows from the analysis described in [19], the temperature which is the most important for the development of puffing and micro-explosion is the temperature at the fuel-water interface. The plots of this temperature versus time for droplets similar to those presented in Fig. 4 are shown in Fig. 6. Stars in this figure show the time instants when the puffing/micro-explosion started. The temperatures at the fuel-water interface were measured at 7 to 10 points in each time instant. The scatter of these measurements did not exceed 15 K.

As follows from Fig. 6, the lead droplet is the first to heat up, followed by the middle droplet and then the downstream droplet. This is consistent with the observed times to puffing/micro-explosion discussed later in this section.

Plots similar to those shown in Fig. 6 were obtained for droplets of 10% Diesel fuel and 90% water. The general shapes of the curves were similar to those shown in Fig. 6. The main difference between the results is that in the case of 10% Diesel fuel, the interface boundary heats up faster due to the thinner fuel film. For identical cases, but different compositions, the difference in time to puffing can reach 1 s. At the same time instants for the same initial condition but different compositions of droplets, differences in temperature at the fuel-water interface can reach 20 K.

Assuming, following [19], that puffing/micro-explosion starts when the temperature at the fuel-water interface reaches the water nucleation temperature, we calculated the degree of superheating (difference between the water nucleation and boiling temperatures: $\Delta T_{SH} = T_N - T_B$) versus heating rate $dT/dt \equiv \dot{T}$ at the fuel/water interface of composite droplets of 90% Diesel fuel and 10% water (lead, middle and downstream). The results are shown in Fig. 7. As follows from this figure, an increase in $\Delta T_{SH}$ agrees well with the correlation suggested in [17]:

$$T_N = T_B + 12 \times \tanh(\dot{T}/50); \qquad 0 \le \dot{T} \le 300 \ \text{K/s}. \tag{1}$$

This correlation is shown as the solid curve in Fig. 7.

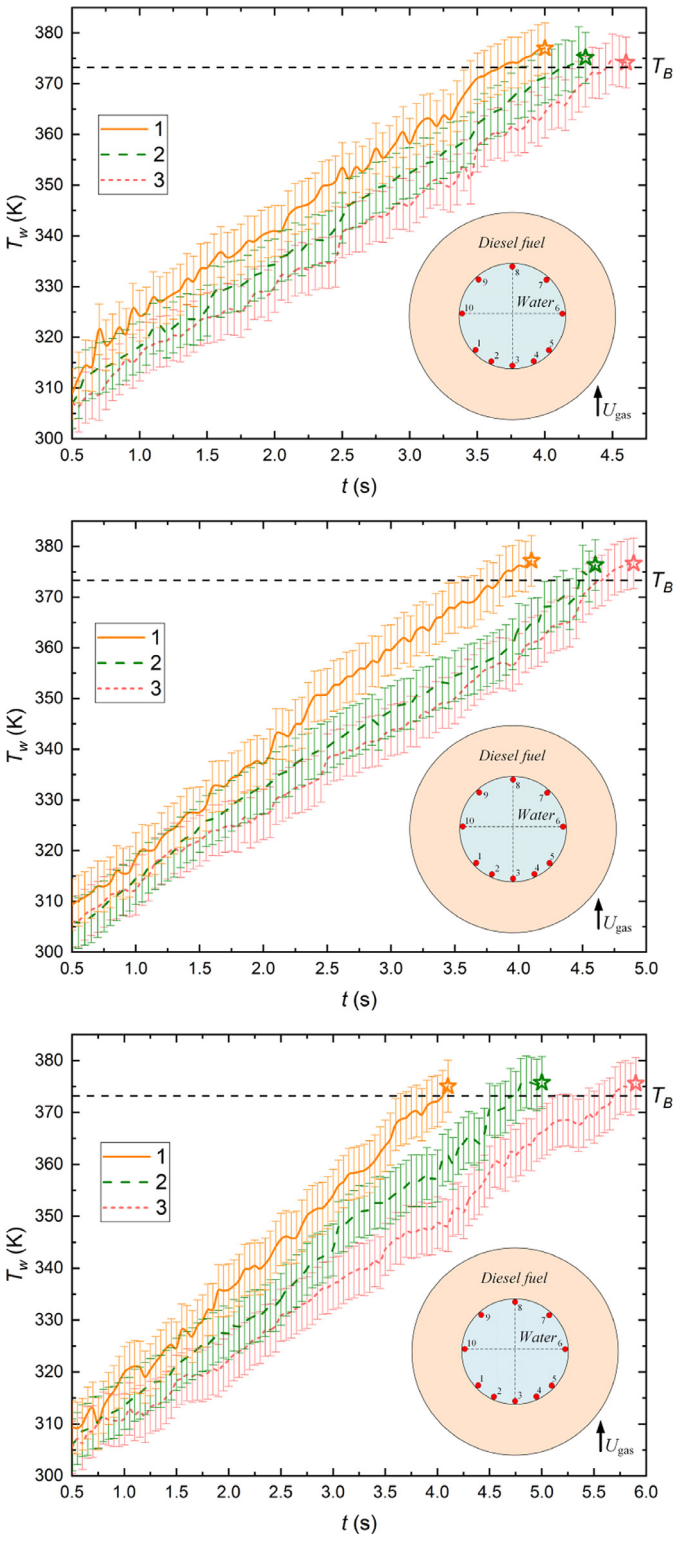


**Fig. 6.** The temperature at the fuel-water interface versus time for the lead (1), middle (2) and downstream (3) droplets of 90% Diesel fuel and 10% water. Top, $L = 9.86 \pm 0.06$ mm and $R_{d0} = 0.88 \pm 0.04$ mm; middle, $L = 6.48 \pm 0.04$ mm and $R_{d0} = 0.89 \pm 0.02$ mm; bottom, $L = 3.55 \pm 0.05$ mm and $R_{d0} = 0.88 \pm 0.02$ mm.

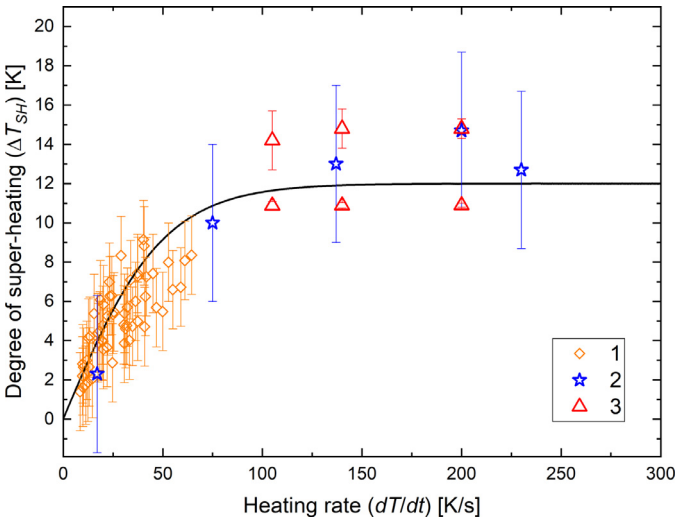


**Fig. 7.** The degree of super-heating ($\Delta T_{SH}$) versus heating rate at the water/fuel interface of droplets of 90% Diesel fuel and 10% water (lead, middle and downstream) inferred from our experiments (1), experiments described in [17] (2) and experiments described in [30] (3). The solid curve shows the correlation predicted by Expression (1).

Results similar to those shown in Fig. 7 for droplets of 90% Diesel fuel and 10% water were obtained for droplets of 10% Diesel fuel and 90% water. These results were also shown to be well approximated by Expression (1).

Plots of time to puffing/micro-explosion ($\tau_p$) for the lead, middle and downstream droplets of 90% Diesel fuel and 10% water versus ambient gas temperature are shown in Fig. 8. As follows from this figure, for all three droplets, $\tau_p$ decreases with temperature as in the case of isolated droplets or two droplets in tandem [19]. $\tau_p$ for the lead droplet is always shorter than it is for the middle and downstream droplets for the whole range of temperatures under consideration.

Plots similar to those shown in Fig. 8 were obtained for droplets of 10% Diesel fuel and 90% water. The main difference between these plots and those shown in Fig. 8 lies in their smaller values of $\tau_p$ (in almost all cases). This difference can be as much as 25%. The higher the temperature, the smaller the difference.

Plots of time to puffing/micro-explosion ($\tau_p$) for the same lead, middle and downstream droplets as in Fig. 8 versus the distance between droplets ($L$) are shown in Fig. 9. As follows from this figure, for all three droplets $\tau_p$ decreases with increasing $L$ as in the case of two droplets in tandem [19]. This decrease is hardly visible for the case of the lead droplet, but fast for the middle and downstream droplets, especially for small $L$.

Plots similar to those shown in Fig. 9 were obtained for droplets of 10% Diesel fuel and 90% water. The main difference between these plots and those shown in Fig. 9 lies in their smaller values of $\tau_p$. This difference could be as much as 20% for the lead droplet and 15% for the middle and downstream droplets. A more pronounced decrease in $\tau_p$ with increasing $L$ for the lead droplet of 10% Diesel fuel and 90% water, compared with that for droplets of 90% Diesel fuel and 10% water, was observed (not shown).

## 4. An overview of the model

### 4.1. Initiation of puffing/micro-explosion

As in our previous paper [19], we assumed that puffing/micro-explosion is initiated when the temperature at the fuel-water interface reaches the water nucleation temperature that is estimated based on Expression (1). As in [18], the effects of external gas

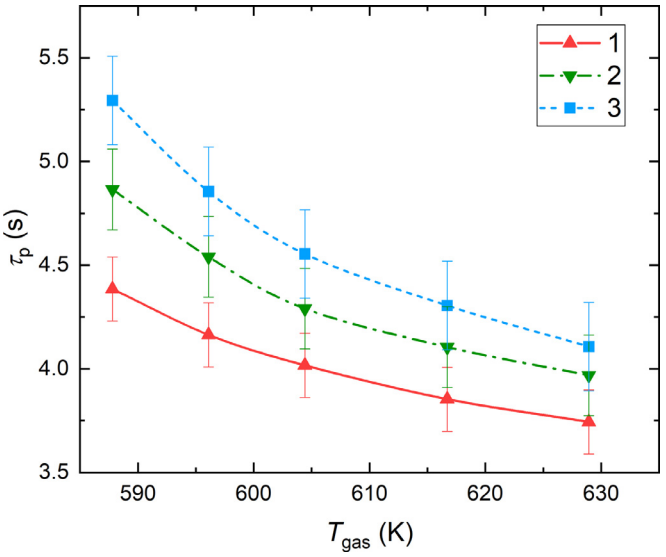


**Fig. 8.** Time to puffing/micro-explosion ($\tau_p$) versus ambient gas temperature for the lead (1), middle (2) and downstream (3) composite droplets (90% volume fraction of Diesel fuel; 10% volume fraction of water). The distances between droplets ($L$) were $9.86 \pm 0.08$ mm and the initial droplet radii $R_{d0}$ were $0.89 \pm 0.04$ mm.

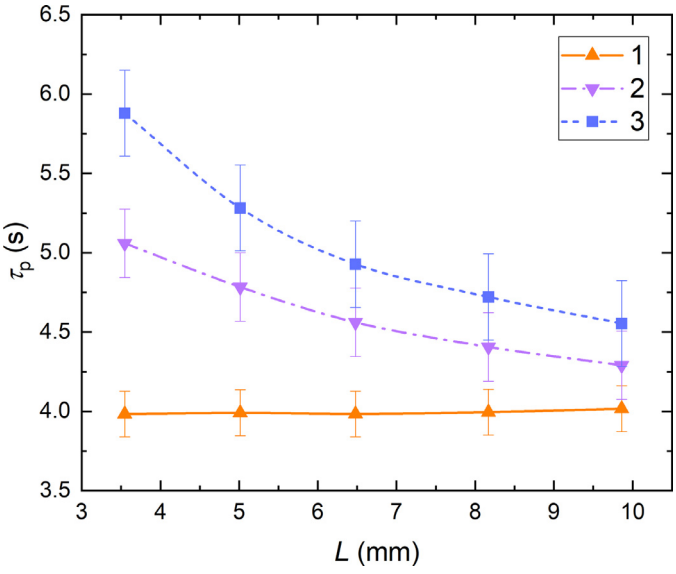


**Fig. 9.** Time to puffing/micro-explosion versus the distance between droplets ($L$) for the lead (1), middle (2) and downstream (3) composite droplets (90% volume fraction of Diesel fuel; 10% volume fraction of water). The ambient gas temperature was $604 \pm 10$ K and the initial droplet radii $R_{d0}$ were $0.89 \pm 0.04$ mm.

flow on the values of Nusselt ($Nu$) and Sherwood ($Sh$) numbers are taken into account but not the effects of this flow on the recirculation inside the droplets. The effect on the puffing/micro-explosion of three droplets in a flow was also attributed to the impact of the external gas flow on the values of $Nu$ and $Sh$. The latter effect was inferred from the analysis of the heat/mass transfer processes during the flow of air around three droplets positioned one behind the other, as described in the following section.

The effect of thermal radiation on puffing/micro-explosion is expected to be insignificant for the range of gas temperatures typical for our experiments (587–629 K) and is ignored in our analysis [29]. As in [19] the effect of support on puffing/micro-explosion is taken into account using the approach suggested in [26].

### 4.2. Flow around three droplets, one behind the other

We carried out a numerical study of the heating and evaporation of three droplets, one behind the other, placed in a flow of air at atmospheric pressure. Our analysis was based on the approach developed in [31] to evaluate heat and mass transfer in a line of evenly spaced droplets and applied in [19] to the analysis of two droplets in tandem.

The average values of $Nu$ and $Sh$ were obtained for the lead, middle and downstream droplets for the values of parameters used in the experiments ($Re$ in the range 5.8 to 6.3, $B_M$ in the range 0.05 to 0.28, $B_T$ in the range 0 to 0.16, $Sc$ in the range 3.5 to 3, $Pr$ in the range 0.77 to 0.76, the distance parameter $C = L/(2R_{d0})$ in the range 2 to 8). The results of calculations are shown in Appendix 1.

As follows from these results (see Appendix 1), the values of $Nu$ and $Sh$ are weak functions of $Re$, $B_M$, $B_T$, $Sc$ and $Pr$ which allowed us to calculate $Nu$ and $Sh$ using the initial values of the input parameters: $Re = 5.82$, $B_M = 0.05$, $B_T = 0.024$, $Sc = 3.52$ and $Pr = 0.7722$. The results of calculations of the correction factors for these numbers, $Nu/Nu_{iso}$ and $Sh/Sh_{iso}$, where $Nu_{iso}$ and $Sh_{iso}$ are Nusselt and Sherwood numbers for isolated droplets, are presented in Fig. 10. Following [19,31], the following formulae were used for estimation of $Nu_{iso}$ and $Sh_{iso}$:

$$Nu_{iso} = 1 + (1 + \alpha Re\, Pr)^{\gamma} \cdot (1 + \delta Re)^{\beta} \quad (2)$$

$$Sh_{iso} = 1 + (1 + \alpha Re\, Sc)^{\gamma} \cdot (1 + \delta Re)^{\beta}, \quad (3)$$

where $\alpha = 1.0024$, $\gamma = 0.3419$, $\beta = 0.0989$ and $\delta = 0.2046$. Note that a deviation of a few per cent could be observed for both $Nu$ and $Sh$ between the results of the numerical simulations and those predicted by the classical models [29].

As follows from Fig. 10, the correction factors are less than 1 and increase with increasing $C$ in all cases. The minimal values for all correction factors are predicted for the downstream droplets. For $C \geq 3$ the correction factors for the lead droplet are indistinguishable from 1 on the plots.

The correction factors shown in Fig. 10 are used in the next section for the analysis of heating/evaporation of composite droplets and the development within them of puffing/micro-explosions.

## 5. Experimental results versus modelling

In this section the results of the application of the model described in Section 4 to the analysis of the experimental results described in Section 3, and the comparison between the simulated and experimental results are presented. The thermodynamic and transport properties of Diesel fuel and distilled water were taken from [32].

In contrast to previous analysis of puffing/micro-explosion, including the one presented in [19], our work focuses not only on the time to puffing/micro-explosion, but also on the time evolution of the temperature at the fuel-water interface before the start of puffing/micro-explosion. The results of our experimental observation of the latter temperature are shown in Fig. 6.

In Fig. 11 we reproduced the experimental results presented in Fig. 6 (without error bars) and added the predicted values of this temperature using the model described in Section 4. As follows from Fig. 11, the general trends of the time evolution of $T_w$ observed experimentally and predicted by the model are similar for all three values of $C$. These include almost linear increase in $T_w$ with time for most of the heating period and smaller rates of increase in $T_w$ for the middle and downstream droplets compared with the lead droplets. This difference between the rates of increase in $T_w$ increases when $C$ decreases.

Although the difference between observed and predicted values of $T_w$ lies within the experimental error bars in most cases,

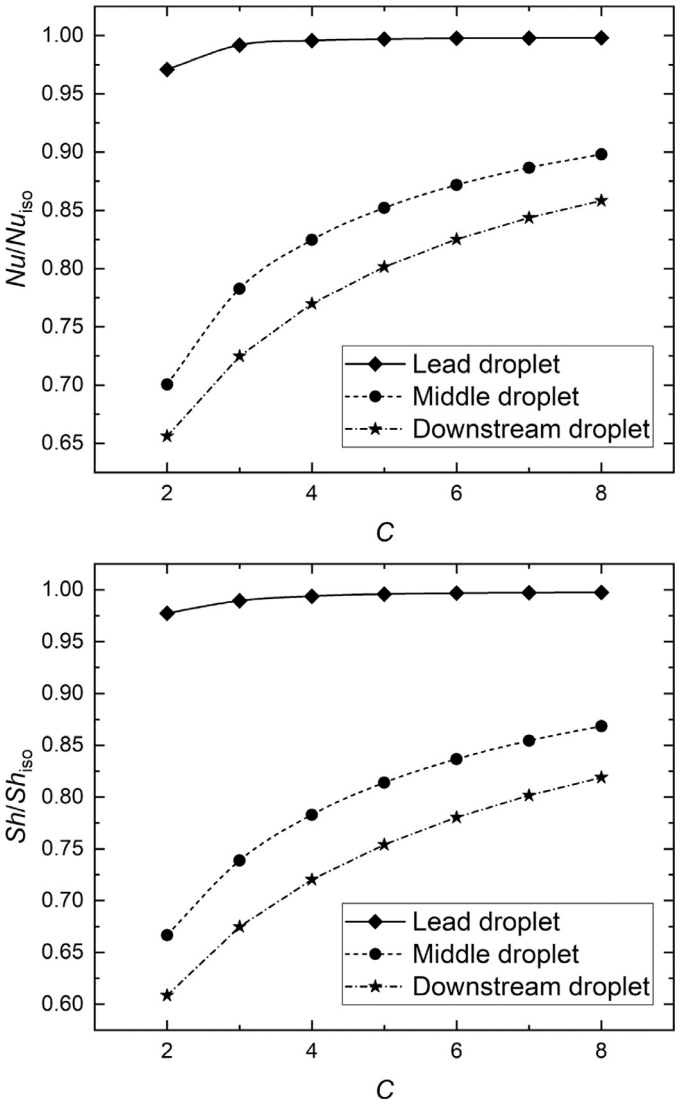


**Fig. 10.** Correction factors for Nusselt and Sherwood numbers, $Nu/Nu_{iso}$ and $Sh/Sh_{iso}$, for the lead, middle and downstream droplets versus the distance parameter $C$.

the observed $T_w$ tend to be larger than those predicted by simulations. This is attributed to the main assumption of the model that a water sub-droplet is located exactly in the centre of the fuel droplet. If we take into account a possible shifting of the water sub-droplet from this centre then we would expect quicker heating of the water-fuel interface in agreement with experimental observations.

In Fig. 12 we reproduced the experimental results presented in Fig. 8 and added the predicted values of this time to puffing/micro-explosion using the model described in Section 4. As follows from Fig. 12, the general trends of the dependence of $\tau_p$ on $T_{gas}$ observed experimentally and predicted by the model are similar for all three droplets. The shortest $\tau_p$ is observed and predicted for the lead droplet. Both experimentally observed and predicted values of $\tau_p$ decrease with increasing $T_{gas}$. Observed and predicted differences in $\tau_p$ for the lead and middle droplets and for the middle and downstream droplets decrease with increasing $T_{gas}$.

At the same time, the observed $\tau_p$ tend to be shorter than the predicted ones. This result is compatible with the trends in $T_w$ shown in Fig. 11 and is attributed to the main assumption of the model that the water sub-droplet is located exactly in the centre of the fuel droplet.

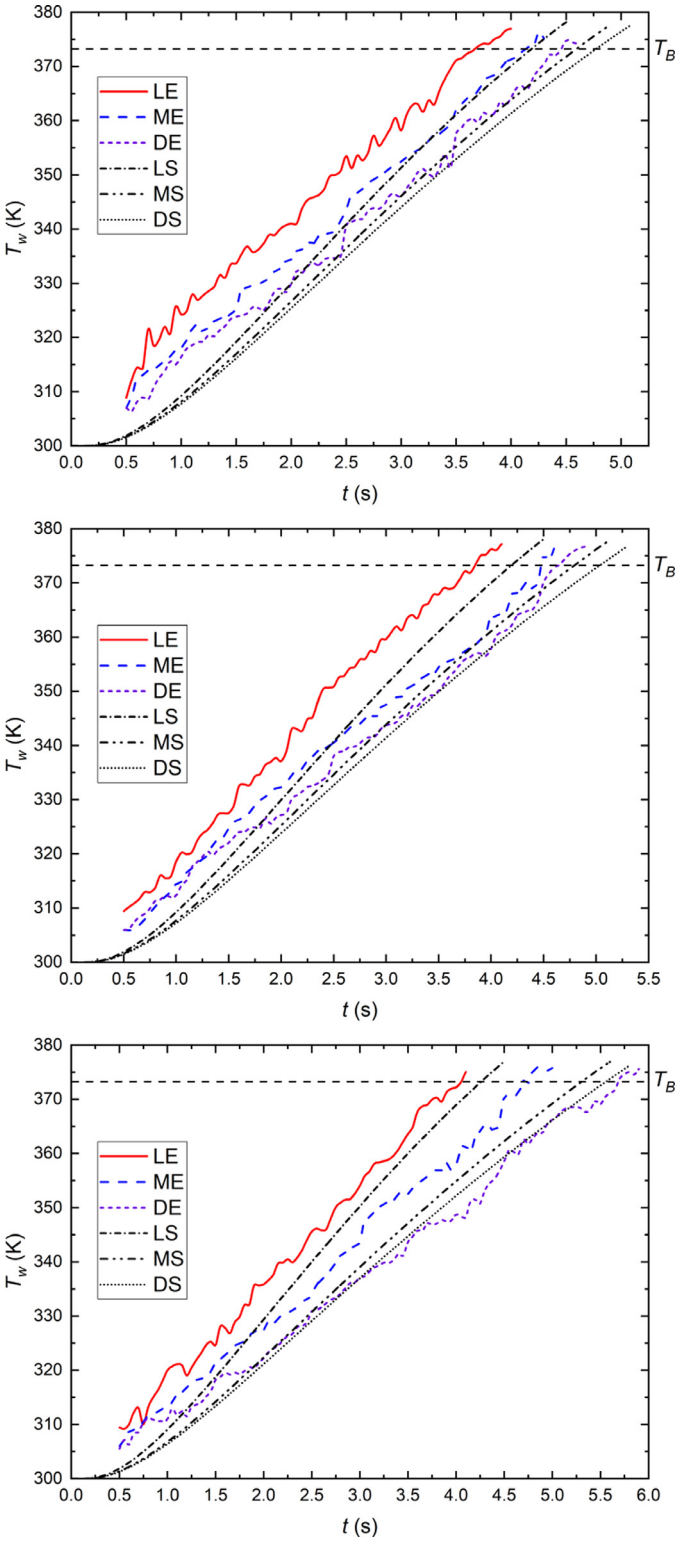


**Fig. 11.** The temperature at the fuel-water interface ($T_w$) observed experimentally (predicted by the simulation) versus time for the lead (LE(LS)), middle (ME(MS)) and downstream (DE(DS)) droplets of 90% Diesel fuel and 10% water. Top, $L = 9.86 \pm 0.06$ mm and $R_{d0} = 0.88 \pm 0.04$ mm ($C = 5.60$); middle, $L = 6.48 \pm 0.04$ mm and $R_{d0} = 0.89 \pm 0.02$ mm ($C = 3.64$); bottom, $L = 3.55 \pm 0.05$ mm and $R_{d0} = 0.88 \pm 0.03$ mm ($C = 2.02$).

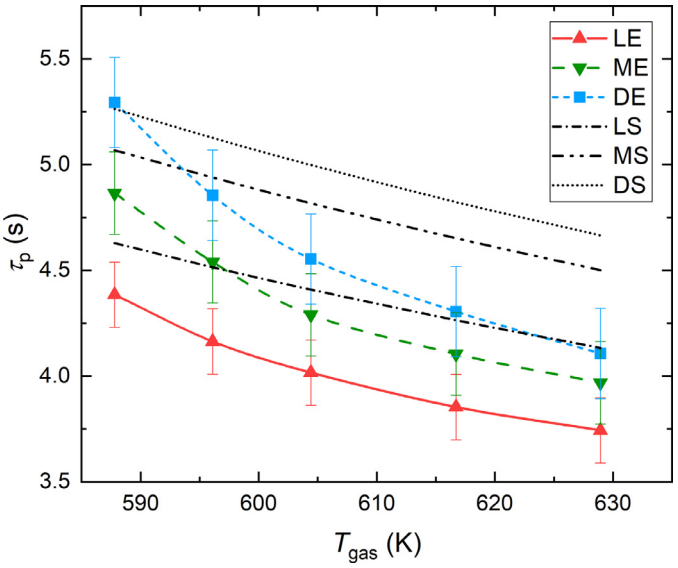


**Fig. 12.** Time to puffing/micro-explosion ($\tau_p$) observed experimentally (predicted by the simulation) versus ambient gas temperature for the lead (LE(LS)), middle (ME(MS)) and downstream (DE(DS)) composite droplets (90% volume fraction of Diesel fuel; 10% volume fraction of water). The distance between droplets ($L$) was $9.86 \pm 0.08$ mm and the initial droplet radii $R_{d0}$ were $0.89 \pm 0.04$ mm (the same as in Fig. 8).

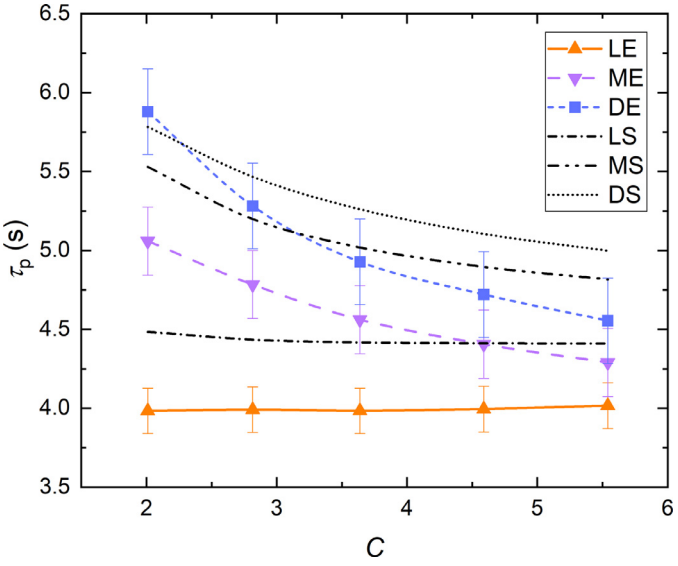


**Fig. 13.** Time to puffing/micro-explosion observed experimentally (predicted by the simulation) versus the distance parameter ($C$) for the lead (LE(LS)), middle (ME(MS)) and downstream (DE(DS)) composite droplets (90% volume fraction of Diesel fuel; 10% volume fraction of water). The ambient gas temperature was $604 \pm 10$ K and the initial droplet radii $R_{d0}$ were $0.89 \pm 0.04$ mm (the same as in Fig. 9).

In Fig. 13 we reproduced the experimental results presented in Fig. 9 and added the predicted values of this time to puffing/micro-explosion using the model described in Section 4. As follows from Fig. 13, the general trends of the dependence of $\tau_p$ on the distance parameter $C$ observed experimentally and predicted by the model are similar for all three droplets. The shortest $\tau_p$ is observed and predicted for the lead droplet. Both experimentally observed and predicted values of $\tau_p$ for the middle and downstream droplets decrease with increasing $C$. Observed and predicted differences in $\tau_p$ for the lead and middle droplets and for the middle and downstream droplet decrease with increasing $C$. As in the cases shown in Figs. 11 and 12, the tendency for the observed $\tau_p$ to be shorter than predicted is attributed to the main limitation of the model used in the analysis, that the water sub-droplet is located in the centre of the fuel droplet.

## 6. Conclusions

The results of experimental and theoretical investigation of the mutual effects of three composite Diesel fuel/water droplets, one behind the other, on their puffing/micro-explosion are presented. The volume fractions of Diesel fuel (water) in the range 10% to 90% (90% to 10%) are investigated although most attention is focused on the case when the volume fraction of Diesel fuel is equal to 90%. The focus of the analysis is not only on finding the time instant when puffing/micro-explosion starts, but also on the investigation of time evolution of temperature at the fuel-water interface before the development of puffing/micro-explosion.

The experimentally observed temperatures at the fuel-water interface are shown to increase almost linearly with time for the lead, middle and downstream droplets. These temperatures were measured at 7 to 10 points in each time instant. The scatter of these measurements did not exceed 15 K. The lead droplet is shown to be the first to heat up, followed by the middle and then the downstream droplet, as expected.

Assuming that puffing/micro-explosion starts when the temperature at the fuel-water interface reaches the water nucleation temperature, the values of the latter temperature as a function of the heating rate are found from the experimental data. The results are shown to be consistent with the earlier suggested correlation for this temperature for all three droplets.

In agreement with the previous results for two droplets in tandem it is found that time to puffing/micro-explosion decreases with increasing gas temperature. It is shown that this time for the lead droplet is always shorter than that of the middle and downstream droplets, and the difference between them decreases as the distance between droplets increases.

The experimental results are interpreted in terms of the previously developed model of fuel/water droplet puffing/micro-explosion, based on the assumptions that the water sub-droplet is located exactly in the centre of the Diesel fuel droplet and that this process is triggered when the temperature at the fuel-water interface reaches the water nucleation temperature. The effect of interaction between lead, middle and downstream droplets is taken into account via modifications to the Nusselt ($Nu$) and Sherwood ($Sh$) numbers for these droplets.

The required modifications to these numbers are obtained based on numerical calculations of the flow and heat/mass transfer processes around three droplets, one behind the other. Using the results of these calculations the dependences of $Nu/Nu_{iso}$ and $Sh/Sh_{iso}$ on the distance parameter $C$ are obtained, where the subscript $_{iso}$ refers to isolated droplets. It is shown that these ratios are weak functions of $Re$, $B_M$, $B_T$, $Pr$ and $Sc$ in the range of values for these parameters typical for these experiments. This allows us to estimate $Nu/Nu_{iso}$ and $Sh/Sh_{iso}$ for the initial values of $Re$, $B_M$, $B_T$, $Pr$ and $Sc$.

The predicted temperatures at the fuel-water interface are shown to be close to those observed experimentally for all three droplets in the distance parameter range 2.02 to 5.60.

As in the previously studied cases of isolated droplets and two droplets in tandem, both experimentally observed and predicted values of the time to puffing/micro-explosion ($\tau_p$) are shown to decrease with increasing $T_{gas}$. Both experimentally observed and predicted values of this time are longer for the middle and downstream droplets than for the lead droplet. The experimentally observed differences in this time for the lead, middle and downstream droplets are close to the predicted values.

## Declaration of Competing Interest

The work described has not been published previously and it is not under consideration for publication elsewhere. Its publication is approved by all authors and tacitly or explicitly by the responsible authorities where the work was carried out. If accepted, it will not be published elsewhere in the same form, in English or in any other language, including electronically without the written consent of the copyright-holder.

## CRediT authorship contribution statement

**D.V. Antonov:** Conceptualization, Methodology, Resources, Investigation, Software, Writing – original draft. **R.S. Volkov:** Resources, Investigation, Software. **R.M. Fedorenko:** Conceptualization, Methodology, Resources, Investigation, Software, Writing – original draft. **P.A. Strizhak:** Supervision, Resources, Investigation, Writing – original draft. **G. Castanet:** Conceptualization, Methodology, Resources, Investigation, Software, Writing – review & editing. **S.S. Sazhin:** Supervision, Methodology, Writing – review & editing.

## Acknowledgements

The authors are grateful: to the National Research Tomsk Polytechnic University (project VIU-ISHFVP-60/2019) which supported P.A. Strizhak (who contributed to the formulation of the problem and analysis of the results) and R.S. Volkov (who contributed to the development of the experimental setup); for scholarships from the President of the Russian Federation (Grants SP-447.2021.1 and MN-7/2260) which supported D. Antonov and R. Fedorenko (who performed the experiments, applied the model to their analysis and prepared the first draft of the paper); to the Université de Lorraine and the Institut Carnot Icéel for the CALICO (Combustion d'Aérosols LIquides Complexes) grant which supported G. Castanet (who contributed to the development of the model, the simulations and preparation of the text of the paper), and to the Russian Science Foundation (Grant 21-19-00876), which supported S.S. Sazhin (who contributed to the development of the model, analysis of the results and preparation of the text of the paper).

## Appemdix A

The determination of the Nusselt and Sherwood numbers for the three droplets positioned one behind the other is based on the same approach as described in [31]. The problem is simplified by considering heat and mass transfers within the gas phase only. The assumptions made are the same as used in the derivation of the $d^2$-law for an isolated droplet. The steady state Navier-Stokes equations, the continuity equation for mass, the convection-diffusion equations for the vapour and heat transfers are solved assuming that the droplet arrangement is axisymmetric. The droplets are assumed to be rigid spheres. Only the normal velocity, corresponding to the Stefan flow, is considered even in the case when Diesel fuel is weakly volatile in the conditions of the experiments. The tangential velocity at the liquid surface is assumed equal to zero. Since only the mean values of the Nusselt and Sherwood numbers are sought from the simulations, other simplifications are also made. Both temperature and vapour concentration are assumed to be uniform over the droplet surface. The finite element method is applied for the numerical solution. It uses an unstructured triangular mesh of increased density near the surface of the droplets (typically, the half perimeter of the droplets is divided into 100 elements of equal size).

Even with the above approximations, a comprehensive study of three droplets in a row would be time-consuming, due to a large number of parameters related to the geometry, surface conditions and flow field. An example of a parametric study, where the distance between droplets, the droplet sizes and the surface conditions are modified, was recently presented in [19], but for a more simple case of two droplets. In the present study, we used experimental results that refer to droplet evolution to limit the scope of investigations. The ranges of $Re$, $C$, $Pr$, $Sc$, $B_M$ and $B_T$ were approximated to determine the influence of these dimensionless numbers on heat and mass transfer under the selected experimental conditions.

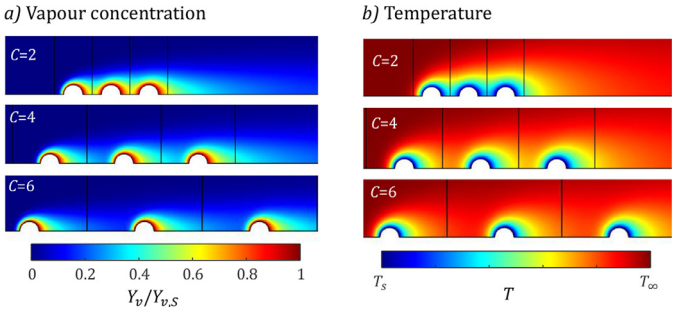


**Fig. A1.** Distributions of temperature and vapour concentration around the three droplets for three values of the distance parameter $C$ ($Re$= 5.8, $Pr$= 0.77, $Sc$=3.52, $B_M$=0.05 and $B_T$=0.024).

Fig. A1 shows the vapour and temperature distributions around the three droplets for $C = 2$, $C = 4$ and $C = 6$. These simulations were performed for values of the parameters relevant to the beginning of the experiments when the surface temperature was about 340 K: $Re$= 5.8, $Pr$= 0.77, $Sc$=3.52, $B_M$=0.05 and $B_T$=0.024. As can be seen in this figure, the spacing between the droplets clearly affects the temperature and vapour distribution around the middle and downstream droplets. Using these temperature and vapour concentration fields, Sherwood and Nusselt numbers were calculated as:

$$Nu = \frac{2R_d}{(T_\infty - T_S)} \left.\frac{\partial T}{\partial R}\right|_{R=R_d}, \tag{A.1}$$

$$Sh = -\frac{2R_d}{(Y_{vS} - Y_{v\infty})} \left.\frac{\partial Y_v}{\partial R}\right|_{R=R_d}, \tag{A.2}$$

where $R$ is the radial coordinate from the centre of the droplet under consideration.

To evaluate the effect of interaction between droplets on heat and mass transfer processes, the Nusselt and Sherwood numbers were averaged over the surface of the droplets and divided by their counterparts for an isolated droplet using Eqs. (2) and (3). The evolution of $Nu/Nu_{iso}$ and $Sh/Sh_{iso}$ is presented in Fig. 10. As expected, a stronger reduction in the heat and mass transfers is observed for the middle and downstream droplets. As the droplets are heated, the conditions at their surfaces change. The heating process was the fastest for the lead droplet, and was almost the same as for an isolated droplet.

A decrease in $Nu$ and $Sh$ of about 6% was observed as a result of heating and evaporation as demonstrated in Fig. A2. The evolutions of $Nu$ and $Sh$ as functions of $C$ follow the same trends at the beginning of the process and just before puffing/micro-explosion starts. Note that the reduced Sherwood and Nusselt numbers, $Sh/Sh_{iso}$ and $Nu/Nu_{iso}$, are only slightly affected by the heating process with variations of less than 0.5%. Therefore, it can be concluded that $Sh/Sh_{iso}$ and $Nu/Nu_{iso}$ are weakly dependent on $Re$, $B_M$, $B_T$, $Pr$ and $Sc$ in the present study. They can be considered as functions of the distance parameter $C$ only. Also, changes in the sizes of the droplets during the experiments can be ignored. This is related

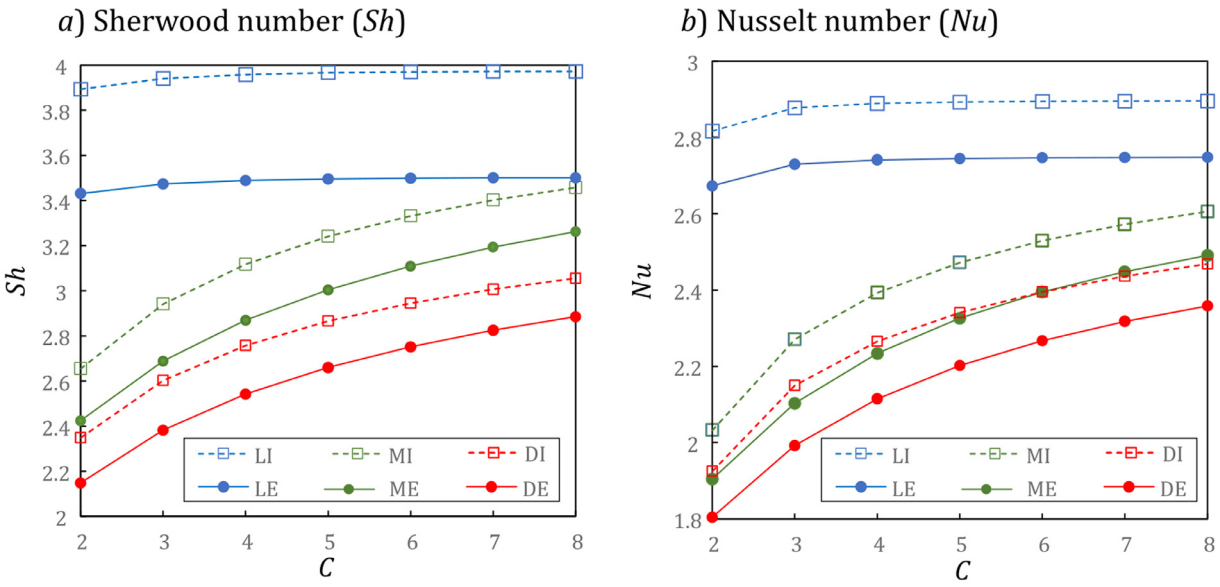


**Fig. A2.** Evolutions of the Nusselt and Sherwood numbers of the string of three droplets at the beginning of the heating process (LI, MI, DI stand for the lead, middle and downstream droplets) and just before puffing or micro-explosion (LE, ME, DE stand for the lead, middle and downstream droplets). The initial conditions: $Re$= 5.8, $Pr$= 0.77, $Sc$=3.52, $B_M$=0.05 and $B_T$=0.02. The conditions just before puffing/micro-explosion: $Re = 6.3$, $B_M = 0.3$, $B_T = 0.16$, $Pr = 0.76$ and $Sc = 2.9$.

to the fact that Diesel fuel is very volatile and thermal expansion compensates for droplet evaporation during the heating phase.

## References


[1] D. Ogunkoya, S. Li, O.J. Rojas, T. Fang, Performance, combustion, and emissions in a diesel engine operated with fuel-in-water emulsions based on lignin, Appl. Energy 154 (2015) 851–861, doi:10.1016/j.apenergy.2015.05.036.

[2] Y. Morozumi, Y. Saito, Effect of physical properties on microexplosion occurrence in water-in-oil emulsion droplets, Energy & Fuels 24 (2010) 1854–1859, doi:10.1021/ef9014026.

[3] C. Cen, H. Wu, C. Lee, L. Fan, F. Liu, Experimental investigation on the sputtering and micro-explosion of emulsion fuel droplets during impact on a heated surfaceInt. J. Heat Mass Transfer 132 (2019) 130-137. doi:10.1016/j.ijheatmasstransfer.2018.12.007.

[4] D.V. Antonov, G.V. Kuznetsov, P.A. Strizhak, Comparison of the characteristics of micro-explosion and ignition of two-fluid water-based droplets, emulsions and suspensions, moving in the high-temperature oxidizer medium, Acta Astronaut 160 (2019) 258–269, doi:10.1016/j.actaastro.2019.04.048.

[5] M.M. Avulapati, L.C. Ganippa, J. Xia, A. Megaritis, Puffing and micro-explosion of diesel-biodiesel-ethanol blends, Fuel 166 (2016) 59–66, doi:10.1016/j.fuel.2015.10.107.

[6] D.V. Antonov, M.V. Piskunov, P.A. Strizhak, Breakup and explosion of droplets of two immiscible fluids and emulsions, Int. J. Thermal Science 142 (2019) 30–41, doi:10.1016/j.ijthermalsci.2019.04.011.

[7] O. Moussa, D. Tarlet, P. Massoli, J. Bellettre, Parametric study of the micro-explosion occurrence of w/o emulsions, Int. J. Thermal Science 133 (2018) 90–97, doi:10.1016/j.ijthermalsci.2018.07.016.

[8] Y. Suzuki, T. Harada, H. Watanabe, M. Shoji, Y. Matsushita, H. H. Aoki, et al., Visualization of aggregation process of dispersed water droplets and the effect of aggregation on secondary atomization of emulsified fuel droplets, Proc. Combust. Inst. 33 (2011) 2063–2070, doi:10.1016/j.proci.2010.05.115.

[9] V. Califano, R. Calabria, P. Massoli, Experimental evaluation of the effect of emulsion stability on micro-explosion phenomena for water-in-oil emulsions, Fuel 117 (2014) 87–94, doi:10.1016/j.fuel.2013.08.073.

[10] J. Shinjo, J. Xia, A. Megaritis, L.C. Ganippa, R.F. Cracknell, Modeling temperature distribution inside an emulsion fuel droplet under convective heating: a key to predicting microexplosion and puffing, At. Sprays 26 (2016) 551–583, doi:10.1615/AtomizSpr.2015013302.

[11] J. Shinjo, J. Xia, L.C. Ganippa, A. Megaritis, Physics of puffing and microexplosion of emulsion fuel droplets, Phys. Fluids 26 (2014) 103302, doi:10.1063/1.4897918.

[12] S. Fostiropoulos, G. Strotos, N. Nikolopoulos, M. Gavaises, Numerical investigation of heavy fuel oil droplet breakup enhancement with water emulsions, Fuel 278 (2020) 118381, doi:10.1016/j.fuel.2020.118381.

[13] O.G. Girin, Dynamics of the emulsified fuel droplet micro-explosion, Atomization Sprays 27 (2017) 407–422, doi:10.1615/AtomizSpr.2017017143.

[14] S.S. Sazhin, O. Rybdylova, C. Crua, M. Heikal, M.A. Ismael, Z. Nissar, A.R.B.A. Aziz, A simple model for puffing/micro-explosions in water-fuel emulsion droplets, Int. J. Heat Mass Transfer 131 (2019) 815–821, doi:10.1016/j.ijheatmasstransfer.2018.11.065.

[15] S. Fostiropoulos, G. Strotos, N. Nikolopoulos, M. Gavaises, A simple model for breakup time prediction of water-heavy fuel oil emulsion droplets, Int. J. Heat Mass Transf 164 (2021) 120581, doi:10.1016/j.ijheatmasstransfer.2020.120581.

[16] D.V. Antonov, R.M. Fedorenko, G.V. Kuznetsov, P.A. Strizhak, Modeling the micro-explosion of miscible and immiscible liquid droplets, Acta Astronaut 171 (2020) 69–82, doi:10.1016/j.actaastro.2020.02.040.

[17] S.S. Sazhin, T. Bar-Kohany, Z. Nissar, D. Antonov, P.A. Strizhak, O.D. Rybdylova, A new approach to modelling micro-explosions in composite droplets, Int. J. Heat and Mass Transfer 161 (2020) 120238, doi:10.1016/j.ijheatmasstransfer.2020.120238.

[18] D.V. Antonov, P.A. Strizhak, R.M. Fedorenko, Z. Nissar, S.S. Sazhin, Puffing/micro-explosion in rapeseed oil/water droplets: The effects of coal micro-particles in water, Fuel 289 (2021) 119814, doi:10.1016/j.fuel.2020.119814.

[19] D.V. Antonov, R.M. Fedorenko, P.A. Strizhak, G. Castanet, S.S. Sazhin, Puffing/micro-explosion of two closely spaced composite droplets in tandem: experimental results and modelling, Int. J. Heat and Mass Transfer 176 (2021) 121449, doi:10.1016/j.ijheatmasstransfer.2021.121449.

[20] C.H. Chiang, W.A. Sirignano, Interacting, convecting, vaporizing fuel droplets with variable properties, Int. J. Heat Mass Transf 36 (1993) 875–886, doi:10.1016/S0017-9310(05)80271-6.

[21] C.H. Chiang, W.A. Sirignano, Asymmetric calculation of three droplet interactions, Atomization Sprays 3 (1993) 91–107, doi:10.1615/AtomizSpr.v3.i1.50.

[22] V. Ayhan, S. Tunca, Experimental investigation on using emulsified fuels with different biofuel additives in a DI diesel engine for performance and emissions, Appl.Therm. Eng. 129 (2018) 841–854, doi:10.1016/j.applthermaleng.2017.10.106.

[23] H.M. Gad, I.A. Ibrahim, M.E. Abdel-baky, A.K.A. El-samed, T.M. Farag, Experimental study of diesel fuel atomization performance of air blast atomizer, exp, Therm. Fluid Sci. 99 (2018) 211–218, doi:10.1016/j.expthermflusci.2018.07.006.

[24] M.A. Shannon, P.W. Bohn, M. Elimelech, J.G. Georgiadis, B.J. Mariñas, A.M. Mayes, Science and technology for water purification in the coming decades, in: Nanosci. Technol., Co-Published with Macmillan Publishers Ltd, UK, 2009, pp. 337–346. Doi: 10.1142/9789814287005_-0035

[25] R.J. Romero, A. Rodriguez-Martinez, Optimal water purification using low grade waste heat in an absorption heat transformer, Desalination 220 (2008) 506–513, doi:10.1016/J.DESAL.2007.05.026.

[26] P.A. Strizhak, R.S. Volkov, G. Castanet, F. Lemoine, O. Rybdylova, S.S. Sazhin, Heating and evaporation of suspended water droplets: experimental studies and modelling, Int. J. Heat and Mass Transfer 127 (2018) 92–106, doi:10.1016/j.ijheatmasstransfer.2018.06.103.

[27] P.P. Tkachenko, N.E. Shlegel, R.S. Volkov, P.A. Strizhak, Experimental study of miscibility of liquids in binary droplet collisions, Chem Eng Res Des 168 (2021) 1–12, doi:10.1016/j.cherd.2021.01.024.

[28] P.A. Strizhak, R.S. Volkov, D.V. Antonov, G. Castanet, S.S. Sazhin, Application of the laser induced phosphorescence method to the analysis of temperature distribution in heated and evaporating droplets, Int. J. Heat Mass Transfer 163 (2020) 120421, doi:10.1016/j.ijheatmasstransfer.2020.120421.

[29] S.S. Sazhin, Droplets and Sprays, 2014 Springer. doi:10.1007/978-1-4471-6386-2.
[30] G.-Y. Su, M. Bucci, T. McKrell, J. Buongiorno, Transient boiling of water under exponentially escalating heat inputs, Part I: Pool boiling, Int. J. Heat and Mass Transf. 96 (2016) 667–684, doi:10.1016/j.ijheatmasstransfer.2016.01.032.
[31] G. Castanet, L. Perrin, O. Caballina, F. Lemoine, Evaporation of closely-spaced interacting droplets arranged in a single row, Int. J. Heat and Mass Transf. 93 (2016) 788–802, doi:10.1016/j.ijheatmasstransfer.2015.09.064.
[32] L. C. Yaws, Yaws handbook of thermodynamic and physical properties of chemical compounds, Knovel, 2003.